10.1177/0003702818811688

Formatted: Font color: Text 1

Article Type: Research Paper

Corresponding author:
Weiliang Xu, 20 Symonds St, Auckland 1010, New Zealand
Email: p.xu@auckland.ac.nz

An Adaptive and Fully Automated Baseline Correction Method for Raman Spectroscopy Based on Morphological Operations and Mollification

Hao Chen[1,2], Weiliang Xu[1,2,*], and Neil G. R. Broderick[3,2]

*Corresponding Author: Weiliang Xu, email: p.xu@auckland.ac.nz

[1]Department of Mechanical Engineering, the University of Auckland, Auckland 1010, New Zealand

[2]The Dodd-Walls Centre for Photonic and Quantum Technologies, PO Box 56, Dunedin 9054, New Zealand

[3]Department of Physics, the University of Auckland, Auckland 1010, New Zealand

Abstract

Baseline drift is a commonly identified and severe problem in Raman spectra, especially for biological samples. The main cause of baseline drift in Raman spectroscopy is fluorescence generated within the sample. If left untreated, it will affect the following qualitative or quantitative analysis. In this paper, an adaptive and fully automated baseline estimation algorithm based on iteratively averaging morphological opening and closing operations is presented. The proposed method is able to deal with different shapes and amplitudes of baselines. It is tested on both simulated and experimental Raman spectra. Comparison of the

proposed method with other morphology-based methods and a well developed penalized least squares-based method is made. The results demonstrate the superior performance of the proposed method and its advantages, in terms of accuracy, adaptivity and computing speed, over other algorithms. In general, this method can also be applied to other spectroscopic data or other types of one-dimensional data.

Keywords: Baseline correction, morphological operations, adaptive, Raman spectroscopy

Introduction

Raman spectroscopy has been established as a powerful analytical tool and applied in various areas including analytical chemistry, biological research, and biomedical study.[1,2] It is able to explore the compositional information of a given sample at the molecular level by detecting inelastically scattered photons which reflects the vibrational modes of chemical bonds in the sample. The advantages of Raman spectroscopy includes its nondestructive nature, high sensitivity, fast speed, and no need of using external markers. However, raw Raman spectra often suffer from strong and irregular baseline drift.[3] This is particularly severe for biological samples which contain abundant fluorophores. If left untreated, the strong baseline drift may affect the results of subsequent qualitative or quantitative analysis. Therefore, it is necessary to perform baseline correction before doing further analysis.

For biological samples, fluorescence is commonly recognized as one of the main sources of baseline drift in Raman spectra. It may be several orders magnitude greater than the detected Raman signal which degrades the quality of measured spectra to a large extent.[4] Many approaches, including instrumental ones and mathematical ones, have been introduced to remove the background interruption. The major techniques of instrumental methods that have been reported are wavelength-shifted excitation[5–7] and time gating techniques,[8–10] which usually require modifications to the existing instruments set-up. The modifications may increase both the complexity and cost of the existing system. Besides, these instrumental methods may not work for in vivo samples due to their fluidity. These drawbacks hinder the widespread use of instrumental baseline correction methods.

On the other hand, mathematical methods have gained their popularity among researchers in the last a few decades. Baselines are estimated using different algorithms directly from recorded spectra with or without user intervention. These methods include polynomial fitting

based methods,[4,11–14] penalized least square based methods,[15–19] first derivative based methods,[20,21] peak detection and interpolation methods,[22] wavelet transform based methods,[23–25] and morphological operations based methods, etc.[3,19,26–28] Polynomial fitting based methods are easy to apply and can effectively remove the baseline. However, a suitable pre-defined polynomial order is of great importance in estimating the baseline. These methods are usually not adaptive and need users to choose a polynomial order. Penalized least square based method, e.g., adaptive iteratively reweighted penalized least squares (airPLS), combine weighted least squares with a penalty item which controls the smoothness of the estimated baseline. Although good results can be obtained using these methods, they still require user intervention to set the optimal parameters. Peak detection based methods involve the procedure of finding the peak location and peak width which cannot be done precisely due to the influence of random noise. Wavelet transform based methods decompose a signal into a user-defined level which is usually decided by visual inspection. The approximation components are removed as they are regarded as the baseline. A drawback of wavelet-based methods is that meaningless negative peaks at the shoulder of Raman peaks often appear.

Mathematical morphology is mainly applied in the field of image processing. It has good performance in extracting features where the shape is the major characteristic. So it is considered to be suitable to analyze one-dimensional signal like Raman spectroscopy. It was first introduced into baseline correction of Raman spectroscopy by Perez-Pueyo et al.[26] They proved the reliability of morphological operators on the removal of baseline in Raman spectra. However, the main shortcomings of their method are: (i) the fitted baseline contains many jumps which are not consistent with the broad and smooth nature of fluorescence background; (ii) distortions of Raman peaks can be identified. A modified version of this method was reported by Chen and Dai[3] by adding an iteration procedure to fit the final baseline gradually. Although improved the result considerably, the estimated baseline is still not smooth, and Raman peaks may not be fully preserved. Koch et al.[27] reported an iterative baseline correction method based on erosion operator and a mollifier. The erosion operation gives a rough estimation of the baseline, and the mollifier smooths the baseline in every iteration. The mollification process also inspires the development of our algorithm.

In this paper, a novel, adaptive, and fully automated baseline correction algorithm based on morphological operations and mollification is proposed. It uses the four basic morphological

operators, i.e., erosion, dilation, opening, and closing, which will be given in detail in the next section. A new averaging operator which combines the four basic operators together is introduced in this study. Without complicated steps like peak detection and stripping, it only utilizes the morphological features of the input spectra and estimates the baseline adaptively and intuitively.

Theory

Mathematical Morphology

Mathematical morphology is a technique mainly used for signal and image processing. It is based on the classic set theory. Its principle is to analyze a set (signal or image) with the help of another set which is called the structuring element. It is suitable for processing signals whose morphological information is the main interest. For two-dimensional signals, e.g., images, the structuring element can be a freeform plane shape. For one-dimensional signal, e.g., spectra, the structuring element can be a window of any width. In this paper, only the one-dimensional implementations of morphological operators are given in detail as correcting the baseline of Raman spectra is our main purpose. Implementations of morphological operators on image processing can be found in the work of Soille.[29]

There are four basic morphological operators in mathematical morphology: erosion, dilation, opening, and closing. Erosion of a spectrum X (a row vector) by a structuring element w can be defined as the following function:

$$Erosion(x_i) = \min(x_{i+j}), j = -l,...,l \quad (1)$$

where x_i is the center point in the structuring element, and l is the half length of the structuring element. The whole length of the structuring element is $2l+1$. Erosion can be regarded as finding the minimum value within a moving window.

Dilation is the complementary operator of the erosion operator. It finds the maximum value within the structuring element and can be defined as:

Formatted: Font color: Text 1
Formatted: Font color: Text 1
Formatted: Font color: Text 1
Formatted: Font color: Text 1
Formatted: Font color: Text 1
Formatted: Font color: Text 1
Formatted: Font color: Text 1
Formatted: Font color: Text 1

$$Dilation(x_i) = \max(x_{i+j}),\ j = -l,...,l \quad (2)$$

Formatted: Font color: Text 1

Formatted: Font color: Text 1

An illustration of the erosion and dilation operation on a simulated spectrum (with a sigmoidal baseline) is given in Figure 1a by a structuring element of 200 points in length. The details of how the simulated spectrum is generated are given in the Experimental section. Peaks that are narrower than the structuring element are effectively diminished by erosion, and the troughs are expanded. The signal after erosion is always lower than or equal to the original. On the contrary, the dilation operator expands the peak regions and narrows the trough regions. And the signal after dilation is always higher than or equal to the original.

The opening operation is a combination of erosion and dilation–erosion results followed by a dilation operation using the same structuring element. Opening smooths the signal nonlinearly and eliminates small features narrower than the structuring element. The opening operation can roughly estimate the baseline of the original signal. However, it distorts almost all the peaks in the original signal. An example is shown in the left enlarged view in Figure 1b. It is defined as:

$$Opening(x_i) = Dilation(Erosion(x_i)) \quad (3)$$

Formatted: Font color: Text 1

Formatted: Font color: Text 1

The complementary operation of opening is closing. It is also a compound operation which is dilation followed by erosion with the same structuring element. The closing operator closes small gaps (or valleys) in the original signal. It may also distort the baseline (e.g., enlarged view on the right in Figure 1b). It is defined as:

$$Closing(x_i) = Erosion(Dilation(x_i)) \quad (4)$$

Formatted: Font color: Text 1

Formatted: Font color: Text 1

The opening and closing operations on the same spectrum are shown in Figure 1b with a structuring element of 200 points in length. Opening and closing are basic morphological operations to extract information from the original signal. Subtracting the opening from the original signal results in peaks information. Subtracting the closing from the original provides its valleys. How well the morphological information can be extracted highly depends on the size of

the structuring element for one-dimensional signals. The optimal size of the structuring element is thought to be at least equal to or slightly larger than the widest peak feature in the original signal. Figure S1 (Supplemental Material) illustrates an example of how the size of the structuring element affects the opening operation.
[Insert Figure 1]

Proposed Baseline Estimation Method

In this study, we introduce a new morphological operator AVG (Eq. 5) which is an average of opening and closing operators as the major morphological operator used in the proposed algorithm. As mentioned previously, although opening and closing have the ability to estimate the baseline roughly, they inevitably distort the peaks or valleys of the original signal. The AVG operator mediates the distortion of opening and closing operators, and the peaks can be significantly suppressed from the original signal. Figure 1c shows the effect of AVG operator and comparison to opening and closing operators.

$$AVG(x_i) = (Opening(x_i) + Closing(x_i))/2 \qquad (5)$$

Formatted: Font color: Text 1

Formatted: Font color: Text 1

As can be seen from Figure 1c, unlike opening operator which removes the peaks almost completely, the AVG operator attenuates peak heights to their half heights approximately and has a relatively moderate estimation in the valleys. Therefore, it can be imagined that, given a suitable structuring element, by adding an iteration procedure, which takes the AVG operation result as the new input of next iteration, the final baseline can be gradually estimated.
The minimum value of the AVG operation result and the original spectrum is taken as the estimated baseline at each iteration. Another fact observed is that one cannot obtain a smooth baseline by simply applying morphological operators. Here, we adopt the mollification process[27] into every iteration to solve this problem. This is done by convolving the estimated baseline in each iteration with a pre-defined mollifier (the size of the mollifier is the same as the structuring element.) Renormalization is needed on the borders when the mollifier runs into void. A mollifier can smooth a signal in its original domain without the need to transform it into a transform domain. After the mollification process, a smooth version of the estimated baseline in

the *i*th iteration is obtained, denoted as $smooth\_b_i(x)$. A positive and symmetric mollifier is selected in this study. The mollifier and the smoothed spectrum are given by Eqs. 6 and 7.

$$M(r) = \begin{cases} \exp(\frac{-1}{1-r^2}) & , r \in (-1,1) \\ 0 & , else \end{cases} \quad (6)$$

$$smoothed\_b_i(x) = \frac{\sum_{k=1}^{n} b_i(k) * M(\frac{x-k}{2l+1})}{\sum_{k=1}^{n} M(\frac{x-k}{2l+1})} \quad (7)$$

where $b_i(x)$ is the estimated baseline, $smooth\_b_i(x)$ is the smoothed baseline, n is the length of the baseline, and 2l+1 is the length of the structuring element.

The iteration procedure is stopped at either the user-defined maximum iteration time is reached, or the relative changing rate[3] (RCR) is lower than a threshold λ. Normally, the value of λ can be between 10^{-3} to 10^{-6}. The RCR in the *i*th iteration is defined as the ratio between the sum square difference of current and last estimated baselines and the sum square of the last estimated baseline (Eq. 8).

$$RCR = \frac{\sum (smooth\_b_i(x) - smooth\_b_{i-1}(x))^2}{\sum smooth\_b_{i-1}(x)^2} \quad (8)$$

To realize fully automated baseline estimation, the optimal size of the structuring element is determined using the method proposed in Perez-Pueyo et al.[26] Briefly, the size of the structuring element is based on the opening operation. This method begins with the shortest structuring element with a length of three points. In each step, the length of the structuring element is increased by two. The openings of the original signal are calculated with the gradually extended structuring element until three consecutive openings are equal. Then, the smallest structuring element used to compute the three equal openings is chosen as the final structuring element and used to estimate the signal baseline.

To better understand the flow of the proposed baseline correction algorithm, key steps are provided as a flowchart in Figure 2.

[Insert Figure 2]

Formatted: Font color: Text 1
Formatted: Font color: Text 1
Formatted: Font color: Text 1
Formatted: Font color: Text 1
Formatted: Font color: Text 1
Formatted: Font color: Text 1
Formatted: Font color: Text 1
Formatted: Font color: Text 1
Formatted: Font color: Text 1
Formatted: Font color: Text 1
Formatted: Font color: Text 1
Formatted: Font color: Text 1

The convergence speed of the proposed method is very fast. It usually takes less than six iterations to reach the final results. Take the previously used spectrum in Figure 1 as an example. The maximum number of iterations is set as 20, and the value of λ is 10^{-4}. Figure 3 shows the baseline estimations at every iteration. The iteration process stops at iteration 3.

[Insert Figure 3]

Experimental

To validate the performance of the proposed baseline estimation method for Raman spectra, a set of simulated spectra and a set of experimental spectra taken from swine backbone (for general consumption) were used. The algorithm development and all data processing in the study were performed in Matlab 2017b (The MathWorks Inc.) under the environment of 64-bit Microsoft Windows 7 with an Intel Core i7-4770 CPU.

Simulated Spectra

The simulated Raman spectra consist of three major components: pure Raman peaks, baseline, and random Gaussian white noise. In order to simulate as many experimental situations as possible, four different types of baseline, including linear, sine, sigmoidal and fourth-order polynomial, are generated. The parameters for generating the four types of baselines are given in supplemental material. The pure Raman peaks are kept all same in each simulated spectrum. The pure Raman peaks are a sum of several Gaussian peaks with a distribution of the following form,

$$p(x) = \frac{A_i}{\delta\sqrt{2\pi}} * exp\left[\frac{-(x-\mu_i)}{2\delta_i^2}\right]^2 \quad (9)$$

Where μ_i is the peak location, δ_i is the standard deviation of each peak, and $\frac{A_i}{\delta\sqrt{2\pi}}$ is the height of each peak. The pure Raman signal is generated intentionally to have individual peaks and overlapping peaks with different intensities and standard deviations. The parameters for generating the pure Raman signal is summarized in Table I. The random noise level is set as 2% of the lowest Raman peak intensity. The pure Raman signal is given in Figure S2**,** and the simulated spectra with different baseline are shown in Figure 4.

Formatted: Font color: Text 1
Formatted: Font color: Text 1
Formatted: Font color: Text 1
Formatted: Font color: Text 1
Formatted: Font color: Text 1
Formatted: Font color: Text 1

Table I. The parameters used to generate Gaussian peaks in the simulated pure Raman spectrum.

Peak ID	A_i	μ_i	δ_i
1	2.8×10^4	200	25
2	3.6×10^4	590	14
3	3×10^4	750	20
4	3×10^4	1000	35
5	4.5×10^4	1400	35
6	8×10^4	1700	30

Formatted: Font color: Text 1
Formatted: Font color: Text 1
Formatted: Font color: Text 1
Formatted: Font color: Text 1
Formatted: Font color: Text 1
Formatted: Font color: Text 1
Formatted: Font color: Text 1
Formatted: Font color: Text 1
Formatted: Font color: Text 1

Experimental Raman Spectra

Raman spectra were taken on swine backbone samples bought from supermarket using a low-resolution fiber optic Raman system. The system has been described somewhere else previously.[30,31] Briefly, it has four major parts: a 785 nm continuous laser source, a fiber optic Raman probe, a spectrometer, and a computer. Thirty spectra of bone tissue and thirty spectra of fatty tissue were measured under 60 mW laser power (at the sample) with 1s integration time. Spectra were all recorded in wavenumber range from around 400 to 3600 cm^{-1}. The spectral resolution of the system is about 36 cm^{-1}. Without intensity normalization, the raw spectra were used to test the performance of the proposed method.

Results and Discussion

Simulated Spectra

In order to illustrate the outstanding performance of the proposed baseline estimation method, two morphology-based methods, MM[27] and I-Mor[3] (Improved-Mor), and a well developed penalized least squares-based method airPLS[17] were also applied to the simulated spectra to make comparisons. The initial morphology-based method Mor[26] was not taken into comparison because I-Mor is an improved version of it. The parameter settings for the methods used to make comparison are as follows: (i) for all morphology-based methods, the size of structuring elements are kept the same as the proposed method; (ii) the RCR values for the proposed method and I-

Mor are both set as 10^{-5}; (iii) for airPLS, the parameter that controls the roughness of the estimated baseline is set as 10^6 for all the simulated spectra, because this value turns out to be suitable for most of the simulated spectra; 4) the maximum number of iterations for I-Mor, MM, airPLS and the proposed method are all set as 20. The four simulated spectra and baseline estimation results using the above methods are shown in Figure 4.

From Figure 4, the four methods all have a very good estimation of the latent baselines in all situations. However, some clear differences are noticeable. I-Mor is only able to estimate the baseline roughly. The estimated baselines of I-Mor in all simulated spectra are all crumpled and have distortion in peak regions. MM has a better performance than I-Mor. However, small bumps in the peak regions can be clearly observed in the estimated baselines. AirPLS is a well-developed method based on penalized least squares. We used a fixed parameter for the penalty item. In most cases, i.e., the linear baseline, the sigmoidal baseline, and the fourth-order polynomial baseline, it works quite well in estimating the baselines. The fitted baselines are smooth and very close to the actual baselines. However, in the case of sine baseline (Figure 4c), some distortion in peak areas can be easily recognized. This can be attributed to the non-adaptive nature of airPLS. In contrast, the proposed method has a nice fitting in all the simulated spectra. The resulted baseline estimations are smooth and very close to the actual baselines. Besides, no deformation of Raman peaks can be observed.

[Insert Figure 4]

The baseline corrected spectra can be easily obtained by applying a top-hat operation, i.e., subtract the estimated baselines from the original spectra. We then simulated 20 spectra of each of the abovementioned type of baseline (80 spectra in total) by varying the noise level from 0.5% to 10% of the lowest simulated Raman peak with a 0.5% step. As the pure simulated Raman signal is known, the root mean squared errors (RMSEs) of each method on different simulated spectra can be calculated. The RMSEs of each algorithm for the four types baselines as the noise level increases from 0.5 % to 10% of the lowest simulated Raman peak are given in Figure 4e to h. It can be easily recognized that the proposed algorithm has the lowest RMSEs in all simulations.

The means and standard errors (SE) of RMSEs of different types of baselines and baseline correction methods are summarized in Table II, and the best results of each column are highlighted in bold. In all simulations, the proposed method has the lowest mean RMSEs among

the above methods. These results demonstrate the outstanding performance of the proposed method.

Table II. The mean and SE of RMSEs of different baseline correction methods on simulated spectra with different types of baselines. Best results in each column are highlighted in bold.

	Linear baseline		Sine baseline		Sigmoidal baseline		Fourth-order polynomial baseline	
	Mean	SE	Mean	SE	Mean	SE	Mean	SE
I-Mor (RMSEs)	79.54	11.91	86.97	11.10	119.47	22.26	84.95	11.33
MM (RMSEs)	43.50	**5.23**	44.46	5.64	43.27	**5.26**	43.18	5.34
airPLS (RMSEs)	59.36	8.66	58.94	7.59	59.39	8.65	56.91	6.88
This paper(RMSEs)	**40.65**	5.39	**43.54**	**5.53**	**40.33**	**5.26**	**40.92**	**5.24**

Formatted: Font color: Text 1
Formatted: Font color: Text 1
Formatted: Font color: Text 1
Formatted: Font color: Text 1
Formatted: Font color: Text 1
Formatted: Font color: Text 1

Experimental Spectra

The proposed method was also applied to real-world Raman spectra taken from swine backbone samples. The raw spectra are only pre-processed with spike removal and noise reduction, and then are processed with the proposed algorithm. The raw and baseline corrected spectra of bone tissue and fatty tissue are shown in Figure 5a and 5b respectively. From visualization, the original spectra of bone tissue suffer much stronger fluorescence (baseline drift) than that of the original spectra of fatty tissue. The fluorescence of bone spectra is extremely strong in the fingerprint region (400 to 1800 cm^{-1}).

As can be seen, the proposed algorithm is able to correct the baseline for all the experimental spectra properly. The baseline corrected spectra show nearly flat baseline and peak features are well preserved. This proves the suitability of this method on spectra with both strong and weak fluorescence contamination. Although without intensity normalization, the baseline corrected spectra of both tissue types show good repetitions.

[Insert Figure 5]

Comparisons with the above-mentioned baseline estimation methods are also made on the experimental spectra. The size of structuring elements of I-Mor and MM is kept the same as the proposed method. The RCR values for the proposed method and I-Mor are both set as 10^{-5}. For airPLS, the parameter that controls the roughness of the estimated baseline is set as 10^6, which is different from the value used for simulated spectra, in order to obtain optimal results.

Again, the maximum number of iterations for all the methods are set as 20. Due to the noise-free Raman spectra are unavailable, the comparison of RMSEs of different baseline correction methods cannot be obtained. Here, we take one representative baseline correction results of each tissue type as an example, and they are provided in Figure 6.

[Insert Figure 6]

As seen in Figure 6a, all four baseline correction methods perform well in approximating the baseline. However, clear differences can be observed. Due to the nature of simple morphological operations, the baseline estimation of I-Mor is not smooth and contains many jumps. Intrusions in peak areas in the finger print region can be seen on the estimated baseline. MM, airPLS, and the proposed method have a similar performance on the selected spectrum. The estimated baseline of MM has a small offset at the range from 2200 to 2700 cm^{-1}. The problem of airPLS is that the parameter that controls the penalty item needs to be tuned in order to attain optimal results. As a fully automated method, our proposed method has a nice and smooth fitting to the baselines except at the left border of the spectrum. The reason may be that the signal after AVG operation is not always lower than the signal before AVG operation. The proposed method retains nearly all the peak features including overlapping peaks.

From Figure 6b, the spectrum of fatty tissue has a relatively lower baseline drift than the bone spectrum. The baseline estimation results of all the methods on the fatty tissue spectrum are quite different to those on the bone spectrum. I-Mor does not have a stable performance on the spectral set of fatty tissue. It only shows a flat estimation in the fingerprint region on some spectra and the reason for this might be the iteration procedure does not stop at a suitable point which continuously drives the fitted baseline moving downwards. The performances of MM and airPLS on the spectra of fatty tissue are similar and better than that of I-Mor. The estimated baselines are smooth. However, they all show certain distortion in the overlapping area from 700 to 1600 cm^{-1}. For MM, the reason might be the convergence is not reached in 20 iterations (maximum iteration). For airPLS, due to the nonadaptive parameters applied, it is not able to find the optimal solutions for all the spectra. By contrast, our proposed method is adaptive and fully automated. It adjusts the size of the structuring element spectrum by spectrum and iteratively fitted to the final baseline. The mollification process in each iteration guarantees the smoothness of the final estimated baseline.

Computing Speed

Under the system environment mentioned in the Experimental section, the computation time of the proposed method for a spectrum of 2000 data points is around 0.1 s to 0.2 s, which ranks the second place among the above-mentioned methods. Its fast calculation speed can be attributed to the fast convergence of the iteration process. The iteration always stops within six iterations on all the tested spectra. AirPLS has the fastest processing speed which is around 0.04 s to 0.1 s per spectrum. Although the proposed method is not the fastest in processing speed, the adaptivity, automation, and accuracy make it a competitive algorithm for base correction in Raman spectra or other spectroscopic data.

Advantages and Disadvantages of the Algorithm

From the above results and discussions, the advantages of the proposed method can be summarized as full automation, adaptivity, and superior performance. Several possible defects of the algorithm can also be identified. First, the estimated baseline might be higher than the spectrum at left and right borders (half size of the structuring element). The reason may be that the minimum value between the original signal and the mollified baseline in each iteration is taken as the input to the next iteration and the AVG operator does not guarantee a signal always lower than the signal before processing. One way to overcome this defect is to discard the borders. Second, in some extreme situation (e.g., SNR is too low), if the optimized size of structuring element is not determined or determined too large by the algorithm, the estimated baseline may not follow the actual signal trend appropriately. Manually selecting the size of the structuring element is expected in this situation. Third, the situation of many overlapping peaks might affect the performance of the proposed method. It may require the user to manually set the structuring element and RCR to obtain the best results.

Conclusion

In this paper, an adaptive and fully automated baseline correction method based morphological operations and mollification has been presented. A new averaging operator which is an average of morphological opening and closing is introduced to baseline correction of Raman spectra. An iteration procedure is applied using the averaging operator to fit the final baseline gradually. A

mollifier is used to obtain a smooth baseline in each iteration. In addition to adaptivity and full automation, the proposed is also fast in calculation speed. The implementation of this method on both simulated spectra with different types of baselines and experimental Raman spectra taken from swine backbone samples proves its good performance. The comparison to other morphology-based method and airPLS also demonstrates its advantages.

Acknowledgment

The first author would like to acknowledge the sponsorship of a doctoral scholarship from the China Scholarship Council.

Funding

This research received no specific grant from any funding agency in the public, commercial, or not-for-profit sectors.

Declaration of Conflicting Interests

The authors declare that there is no conflict of interest.

Supplemental Material
All supplemental material mentioned in the text is available in the online version of the journal.

References

1. D. Cialla-May, X. Zheng, K. Weber, et al. "Recent Progress in Surface-Enhanced Raman Spectroscopy for Biological and Biomedical Applications: From Cells to Clinics". Chem. Soc. Rev. 2017. 46(13): 3945–3961.
2. M. Ledinský, P. Löper, B. Niesen, et al. "Raman Spectroscopy of Organic–Inorganic Halide Perovskite". J. Phys. Chem. Lett. 2015. 6(3): 401–406.
3. Y. Chen, L. Dai. "An Automated Baseline Correction Method Based on Iterative Morphological Operations". Appl. Spectrosc. 2018. 72(5): 731–739.

4. C.A. Lieber, A. Mahadevan-Jansen. "Automated Method for Subtraction of Fluorescence from Biological Raman Spectra". Appl. Spectrosc. 2003. 57(11): 1363–1367.
5. M.T. Gebrekidan, C. Knipfer, F. Stelzle, et al. "A Shifted-Excitation Raman Difference Spectroscopy (SERDS) Evaluation Strategy for the Efficient Isolation of Raman Spectra from Extreme Fluorescence Interference". J. Raman Spectrosc. 2016. 47(2): 198–209.
6. S.T. McCain, R.M. Willett, D.J. Brady. "Multi-Excitation Raman Spectroscopy Technique for Fluorescence Rejection". Opt. Express. 2008. 16(15): 10975–10991.
7. A.C. De Luca, K. Dholakia, M. Mazilu. "Modulated Raman Spectroscopy for Enhanced Cancer Diagnosis at the Cellular Level". Sensors. 2015. 15(6): 13680–13704.
8. E.R. Draper, M.D. Morris, N.P. Camacho, et al. "Novel Assessment of Bone Using Time-Resolved Transcutaneous Raman Spectroscopy". J. Bone Miner. Res. 2005. 20(11): 1968–1972.
9. P. Matousek, M. Towrie, A. Stanley, et al. "Efficient Rejection of Fluorescence from Raman Spectra Using Picosecond Kerr Gating". Appl. Spectrosc. 1999. 53(12): 1485–1489.
10. M.D. Morris, P. Matousek, M. Towrie, et al. "Kerr-Gated Time-Resolved Raman Spectroscopy of Equine Cortical Bone Tissue". J. Biomed. Opt. 2005. 10(1): 014014.
11. P. Cadusch, M. Hlaing, S. Wade, et al. "Improved Methods for Fluorescence Background Subtraction from Raman Spectra". J. Raman Spectrosc. 2013. 44(11): 1587–1595.
12. J. Zhao, H. Lui, D.I. McLean, et al. "Automated Autofluorescence Background Subtraction Algorithm for Biomedical Raman Spectroscopy". Appl. Spectrosc. 2007. 61(11): 1225–1232.
13. J. Liu, J. Sun, X. Huang, et al. "Goldindec: A Novel Algorithm for Raman Spectrum Baseline Correction". Appl. Spectrosc. 2015. 69(7): 834–842.
14. C. Gallo, V. Capozzi, M. Lasalvia, et al. "An Algorithm for Estimation of Background Signal of Raman Spectra from Biological Cell Samples Using Polynomial Functions of Different Degrees". Vib. Spectrosc. 2016. 83: 132–137.
15. S. Baek, A. Park, Y. Ahn, et al. "Baseline Correction Using Asymmetrically Reweighted Penalized Least Squares Smoothing". Analyst. 2015. 140(1): 250–257.
16. J. Peng, S. Peng, A. Jiang, et al. "Asymmetric Least Squares for Multiple Spectra Baseline Correction". Anal. Chim. Acta. 2010. 683(1): 63–68.

17. Z. Zhang, S. Chen, Y. Liang. "Baseline Correction Using Adaptive Iteratively Reweighted Penalized Least Squares". Analyst. 2010. 135(5): 1138–1146.
18. Z. Zhang, S. Chen, Y. Liang, et al. "An Intelligent Background-Correction Algorithm for Highly Fluorescent Samples in Raman Spectroscopy". J. Raman Spectrosc. 2010. 41(6): 659–669.
19. Z. Li, D. Zhan, J. Wang, et al. "Morphological Weighted Penalized Least Squares for Background Correction". Analyst 2013. 138(16): 4483–4492.
20. S. Baek, A. Park, J. Kim, et al. "A Simple Background Elimination Method for Raman Spectra". Chemom. Intell. Lab. Syst. 2009. 98(1): 24–30.
21. Y. Xie, L. Yang, X. Sun, et al. "An Auto-Adaptive Background Subtraction Method for Raman Spectra". Spectrochim. Acta, Part A. 2016. 161: 58–63.
22. L.G. Johnsen, T. Skov, U. Houlberg, et al. "An Automated Method for Baseline Correction, Peak Finding and Peak Grouping in Chromatographic Data". Analyst. 2013. 138(12): 3502–3511.
23. J. Li, L. Choo-Smith, Z. Tang, et al. "Background Removal from Polarized Raman Spectra of Tooth Enamel Using the Wavelet Transform". J. Raman Spectrosc. 2011. 42(4): 580–585.
24. Y. Liu, W. Cai, X. Shao. "Intelligent Background Correction Using an Adaptive Lifting Wavelet". Chemom. Intell. Lab. Syst. 2013. 125: 11–17.
25. D. Chen, Z. Chen, E. Grant. "Adaptive Wavelet Transform Suppresses Background and Noise for Quantitative Analysis by Raman Spectrometry". Anal. Bioanal. Chem. 2011. 400(2): 625–634.
26. R. Perez-Pueyo, M.J. Soneira, S. Ruiz-Moreno. "Morphology-Based Automated Baseline Removal for Raman Spectra of Artistic Pigments". Appl. Spectrosc. 2010. 64(6): 595–600.
27. M. Koch, C. Suhr, B. Roth, et al. "Iterative Morphological and Mollifier-Based Baseline Correction for Raman Spectra". J. Raman Spectrosc. 2017. 48(2): 336–342.
28. H. Liu, Z. Zhang, S. Liu, et al. "Joint Baseline-Correction and Denoising for Raman Spectra". Appl. Spectrosc. 2015. 69(9): 1013–1022.
29. P. Soille. Morphological Image Analysis: Principles and Applications. Berlin; Heidelberg: Springer, 2013.

30. H. Chen, W. Xu, N. Broderick, et al. "An Adaptive Denoising Method for Raman Spectroscopy Based on Lifting Wavelet Transform". J. Raman Spectrosc. 2018. 49(9): 1529–1539.
31. H. Chen, X. Li, N. Broderick, Y. Liu, Y. Zhou, J. Han, W. Xu. "Identification and Characterization of Bladder Cancer by Low-Resolution Fiber-Optic Raman Spectroscopy". J. Biophotonics. 2018. 11(9): e201800016.

Captions

Figure 1. Four basic morphological operations: (a) erosion and dilation; (b) opening and closing with enlarged views; (c) the AVG operator and comparison to the opening and closing. The left enlarged view in (b) shows the distortion of a peak by the opening operation. The right enlarged view in (b) shows the distortion of a valley by closing operation.

Figure 2. Flowchart of the proposed method.

Figure 3. Baseline estimations of the example spectrum at each iteration.

Figure 4. Comparison of different baseline correction methods on the simulated spectra: (a) linear baseline; (b) sine baseline; (c) sigmoidal baseline; (d) fourth-order polynomial. Baseline; (e) to (h) RMSEs of each algorithm for the four types baselines as the noise level increases from 0.5% to 10% of the lowest simulated Raman peak.

Figure 5. Original and baseline corrected experimental spectra: (a) bone tissue of swine backbone; (b) fatty tissue of swine backbone.

Figure 6. Example baseline estimation results using I-Mor, MM, airPLS, and the proposed method on (a) a bone spectrum and (b) a fatty tissue spectrum.

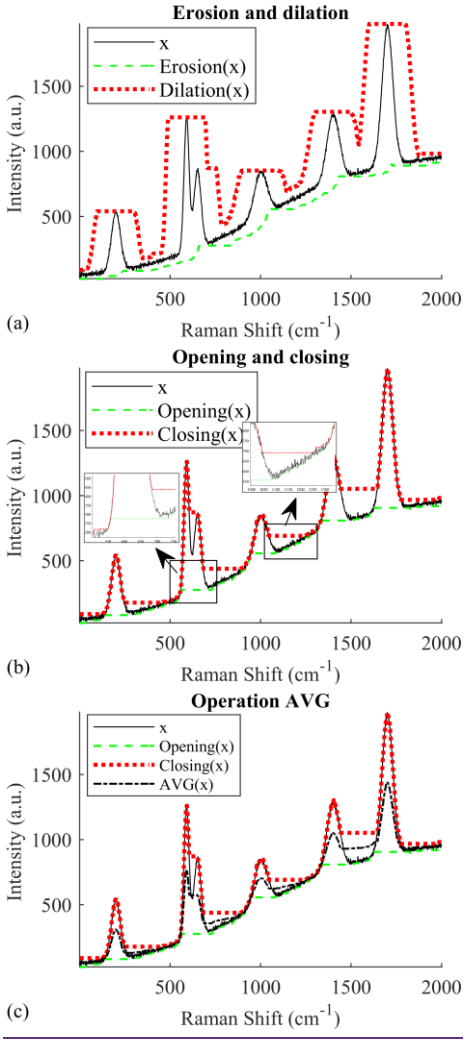
Erosion and dilation
x
Erosion(x)
Dilation(x)
Intensity (a.u.)
Raman Shift (cm-1)
(a)
Opening and closing
x
Opening(x)
Closing(x)
Intensity (a.u.)
Raman Shift (cm-1)
(b)
Operation AVG
x
Opening(x)
Closing(x)
AVG(x)
Intensity (a.u.)
Raman Shift (cm-1)
(c)

Fig 1.

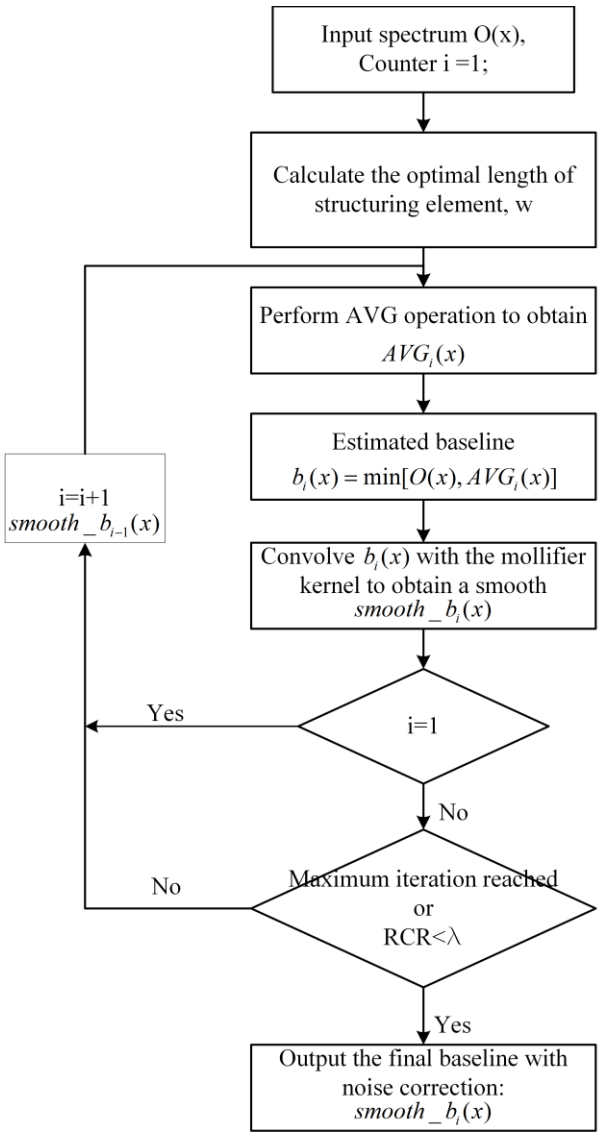
Input spectrum O(x),
Counter i =1;
Calculate the optimal length of structuring element, w
Perform AVG operation to obtain $AVG_i(x)$
Estimated baseline $b_i(x) = \min[O(x), AVG_i(x)]$
Convolve $b_i(x)$ with the mollifier kernel to obtain a smooth $smooth\_b_i(x)$
i=1
Yes
i=i+1
$smooth\_b_{i-1}(x)$
No
Maximum iteration reached or RCR<λ
No
Yes
Output the final baseline with noise correction: $smooth\_b_i(x)$

Fig. 2

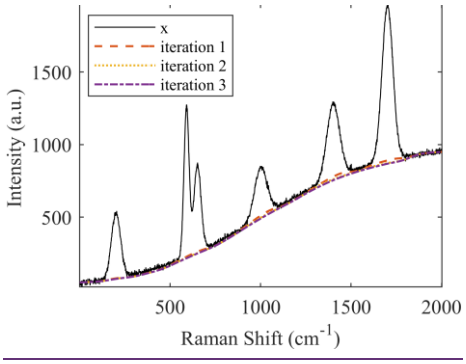
x
iteration 1
iteration 2
iteration 3
Intensity (a.u.)
1500
1000
500
500
1000
1500
2000
Raman Shift (cm-1)

Fig 3.

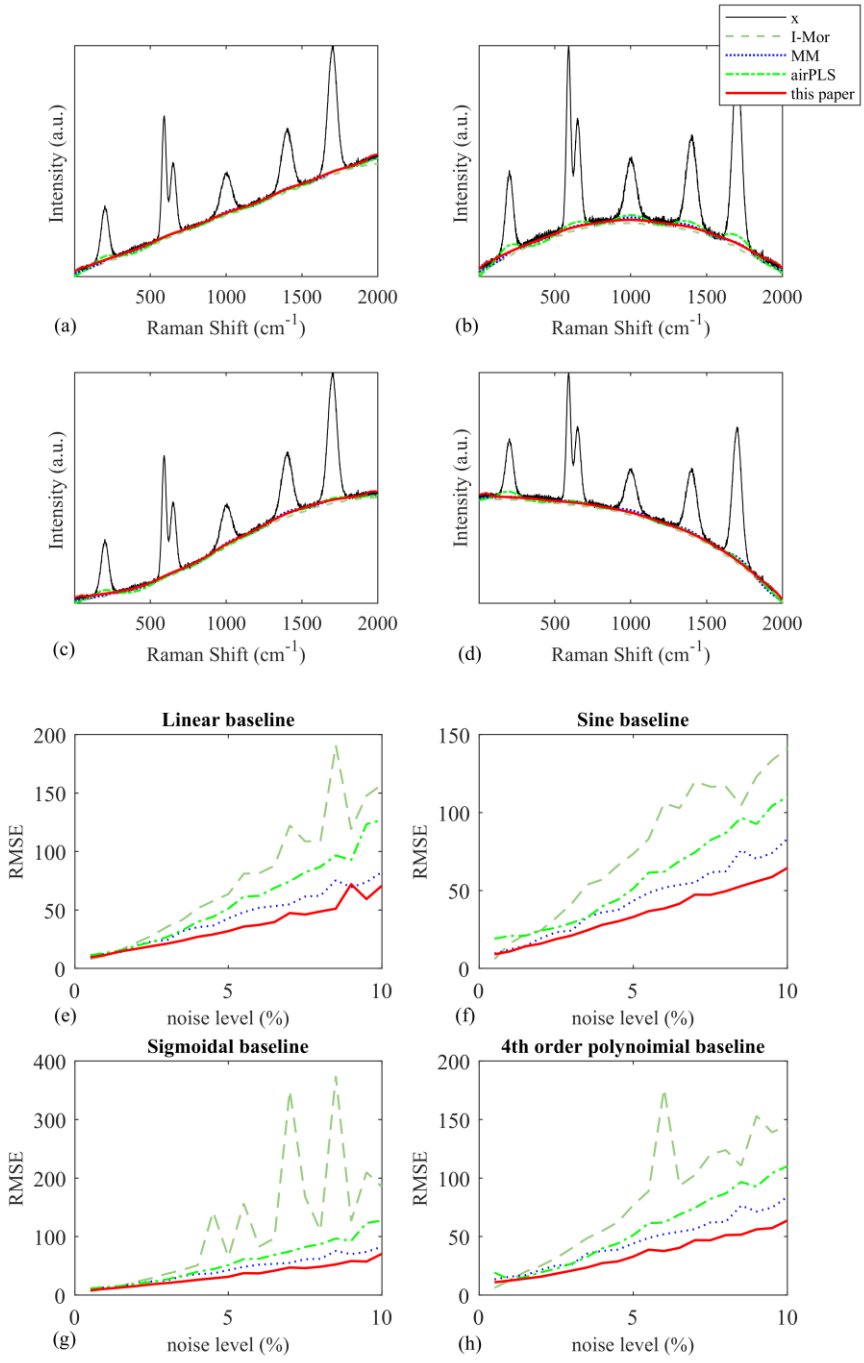
x
I-Mor
MM
airPLS
this paper
Intensity (a.u.)
Raman Shift (cm-1)
(a)
(b)
(c)
(d)
Linear baseline
Sine baseline
Sigmoidal baseline
4th order polynoimial baseline
RMSE
noise level (%)
(e)
(f)
(g)
(h)

Fig 4.

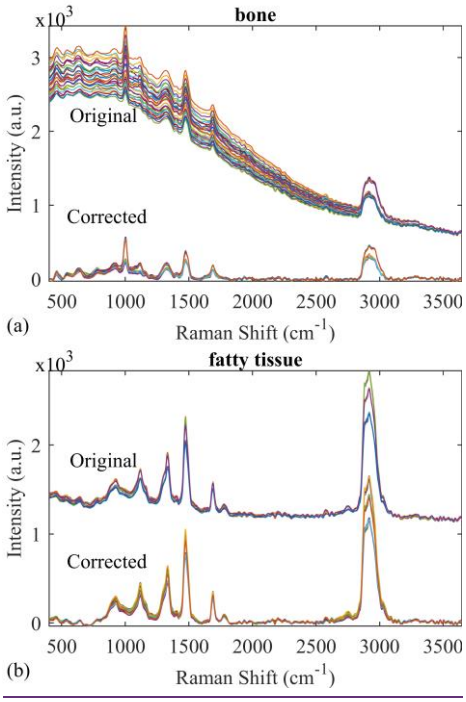
bone
x10^3
3
2
1
0
Intensity (a.u.)
Original
Corrected
500 1000 1500 2000 2500 3000 3500
Raman Shift (cm^-1)
(a)
fatty tissue
x10^3
2
1
0
Intensity (a.u.)
Original
Corrected
500 1000 1500 2000 2500 3000 3500
Raman Shift (cm^-1)
(b)

Fig 5.

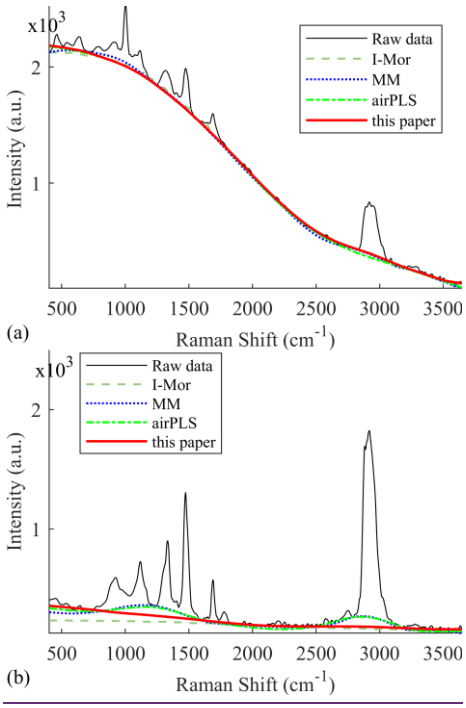

Fig 6.

SUPPLEMENTAL MATERIAL

An adaptive and fully-automated baseline correction method for Raman spectroscopy based on morphological operations and mollification

Hao Chen[1,2], Weiliang Xu[1,2,*], and Neil G. R. Broderick[3,2]
*Corresponding Author: Weiliang Xu, email: p.xu@auckland.ac.nz
[1]Department of Mechanical Engineering, the University of Auckland, Auckland 1010, New Zealand
[2]The Dodd-Walls Centre for Photonic and Quantum Technologies, PO Box 56, Dunedin 9054, New Zealand
[3]Department of Physics, the University of Auckland, Auckland 1010, New Zealand

The four types of baselines described in the paper are generated using the following equations:
1) linear baseline:

$baseline_l = 0.5 \times r, \quad r \in [0, 2000]$

2) sine baseline:

$$baseline_{\sin} = 1000 \times \sin(\frac{(r+1000)\pi}{1000}), \ r \in [0, 2000]$$

3) sigmoidal baseline:

$$baseline_{sig} = \frac{1000}{1+e^{-0.03(r-1000)}}, \quad r \in [0, 2000]$$

4) 4th order polynomial baseline:

$$baseline_p = 80.5 + 0.001519 \times r + 1.6625 \times 10^{-5} \times r^2 + 6.39 * 10^{-9} \times r^3 - 4.6105 \times 10^{-12} \times r^4, \ r \in [0, 2000]$$

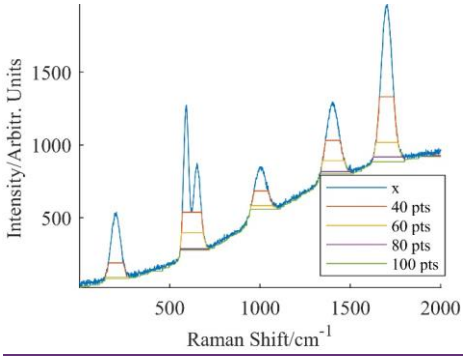

Figure S1 The influence of selected structuring element size on the opening operation

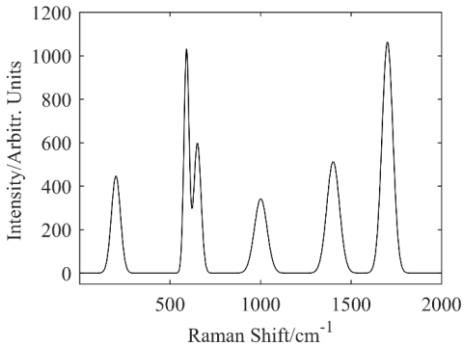

Figure S2 The pure Raman signal generated with Gaussian peaks.